Title

A Bone Density Based Finite Element Study of the Efficacy of Maxillary Protraction Protocols With and Without Mini-Implants

Author

Chu, Howard

Publication Date

2015

Peer reviewed|Thesis/dissertation

UNIVERSITY OF CALIFORNIA
Los Angeles

A Bone Density Based Finite Element Study of the Efficacy of Maxillary Protraction Protocols With and Without Mini-Implants

A thesis submitted in partial satisfaction

of the requirements for the degree Master of Science

in Oral Biology

by

Howard Chu

2015

ABSTRACT OF THE THESIS

A Bone Density Based Finite Element Study of the Efficacy of Maxillary Protraction Protocols With and Without Mini-Implants

By

Howard Chu

Master of Science in Oral Biology

University of California, Los Angeles 2015

Professor Won Moon, Co-chair

Professor Sotirios Tetradis, Co-chair

Objectives: The purpose of this study was to develop a geometrically accurate and adaptable finite element head model for orthodontic and orthopedic simulations. This finite element head model will use a grayscale conversion and image-based meshing method to apply anatomically accurate bone densities of the human skull and craniofacial sutures. The model can then be used to simulate different clinical maxillary protraction protocols using a

conventional facemask appliance and a mico-implant assisted rapid palatal expander (MARPE). Our goal was to improve upon the existing finite element model and to analyze how a bone and suture density based human skull model can improve the analysis of the skeletal effects of these two clinical treatment protocols.

Methods: A 3-dimensional cranial mesh model with associated circummaxillary sutures was developed from CT images and Simpleware modeling software. Using a novel image-based meshing approach rather than the conventional computer-aided design (CAD) approach, the different regions of interests such as bone and sutures are separated into different masks. These masked are defined based on the image grayscale within the region of interest. Mesh generation was completed using a multi-part Extended Volumetric Marching Cubes (EVOMAC) approach where voxels are converted directly into finite elements. The material properties of the craniofacial bone and sutures were extracted from the underlying grayscale intensity Hounsfield (HU) of the CT image. Utilizing ANSYS simulation software, two different maxillary protraction protocols including conventional facemask therapy and micro-implant assisted rapid palatal expander (MARPE) were simulated. The stress distribution and displacement of these two different protraction protocols were analyzed. Superimpositions and video animations were generated to visualize the skeletal effects and to compare the results from the newly generated image-based finite element mesh model with the previous CAD-based mesh model generated from the Mimics software.

Results: Both the newly designed image-based finite element mesh model and the previous CAD-based mesh model produced similar results in regards to direction of maxillary protraction: Conventional facemask results in counter-clockwise rotation of the maxillary complex. In contrast, facemask with the use of micro-implant assisted rapid palatal expander

(MARPE) produces translation of the maxilla in a downward and forward direction. However, the newly designed image-based finite element mesh model produced less magnitudes of movement and less mesh deformation.

Conclusion: The newly generated image-based finite element mesh model produced more clinically accurate results compared to the previous CAD-based mesh model. While the direction of the maxillary movement for the two different protocols is the same for both models, the geometrically accurate bone and suture density based model produced less mesh deformation and more accurately represents actual clinical outcomes. Further maxillary protraction protocols can be tested with this newly developed finite element mesh model.

The thesis of Howard Chu is approved.

Ki-Hyuk Shin

Reuben Kim

Sotirios Tetradis, Co-chair

Won Moon, Co-chair

University of California, Los Angeles

2015

Dedication

I dedicate this thesis to my wife, Christine, for her unconditional love and endless encouragement throughout my training to become an orthodontist. Thank you for always putting me first and for being there for me! Also, I want to dedicate this thesis to my loving parents, Nancy and Henry, for believing in me and supporting me all my life. I love you all.

.

TABLE OF CONTENTS

Acknowledgements

I am so unbelievably grateful for my mentor, Dr. Won Moon, who has guided me throughout every step of this research project and through my clinical training as an orthodontist. I have learned so much from him not only in terms of orthodontics, but also in regards to many important life lessons. I am truly blessed to have worked with Dr. Moon and look forward to many future adventures together.

In addition, I am extremely grateful for Dr. George Youssef and Dr. Ehab Bar for their constant support and guidance. This research project would not have been possible without their selfless contributions.

Introduction

A. Conventional Facemask Therapy

A class III malocclusion, known colloquially as an "underbite", affects nearly 10% in whites and 19% in Asians and is one of the more common facial deformities[1]. Patients with this type of malocclusion often presents with a concave profile, retrusive paranasal region, lower incisor display on smile, protruded lower lip and a prominent chin[2]. Before the 1970s, many clinicians believed that a skeletal class III skeletal malocclusion was primarily a problem with mandibular overgrowth. As such, these clinicians would defer orthodontic treatment until growth of the patient was approaching and treat the patient with a combination of orthodontics and orthognathic surgery[3,4]. However, this would subject the patient to a socially and functionally handicapping malocclusion through their teenage years.

Nanda et al showed that the etiology of a class III skeletal malocclusion can be due to a maxillary skeletal deficiency, mandibular skeletal prognathism, or a combination of the two. Furthermore, Chang et al showed that maxillary hypoplasia is actually the primary etiology of many skeletal class III malocclusions and occurs in 65-67% of cases[1,4]. These studies showed that many patients who appeared skeletally class III in fact had a normal positioned skeletal mandible and they only appeared to have a large mandible due to a deficient maxilla. As such, orthodontic researchers began to focus on treatment that could protract the maxilla downward and forward to reduce the relative protrusion of the mandible.

Studies have shown that young patients with class III skeletal malocclusions can be treated with fairly high predictability with a conventional facemask appliance using dental

anchorage (Figure 1) [5,6]. Using maxillary protraction headgear with tooth-borne anchorage in these young growing patients, clinical studies have shown that 4mm of maxillary advancement can be predictably achieved within 8-12 months[3,7,5]. The overall effects of this treatment include the forward movement of the maxilla, labial tipping of the maxillary incisors, downward and backward rotation of the mandible and lingual tipping of the mandibular incisors. [6,8–12]

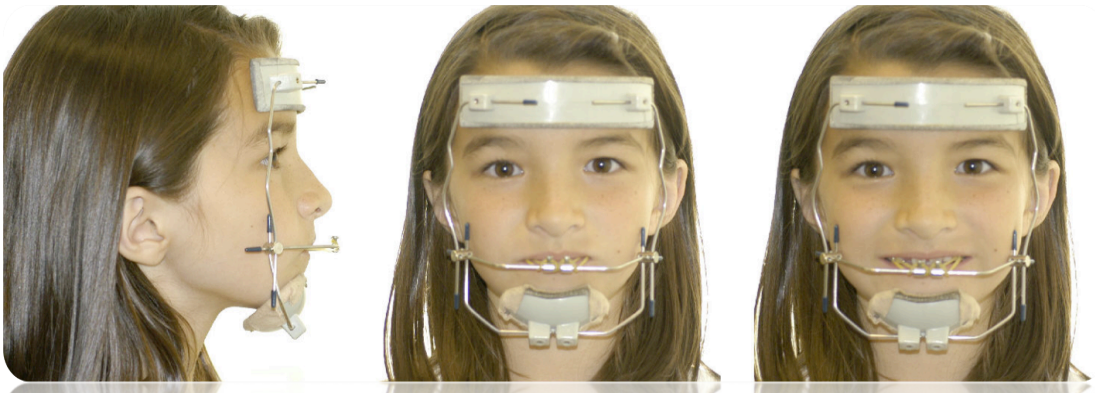

Figure 1. Conventional Facemask Appliance

There are many side-effects when using traditional facemask therapy, where anchorage is achieved using the dentition. With tooth-borne anchorage, forces are applied mainly to the periodontal ligament, not to the maxilla[13]. When more force is being applied to the dentition, skeletal effects are minimal and become secondary to the dental side-effects. Common dental complications resulting from conventional facemask use include proclination of maxillary incisors, extrusion and mesial movement of maxillary molars, retroclination of mandibular incisors, and buccal tipping of maxillary posterior dentition[6,8]. These dental side-effects negatively impact the overarching goal of correcting maxillary and mandibular jaw discrepancies[14].

Many other studies have found that loss of anchorage is another common side-effect of traditional facemask therapy. This becomes a problem since arch preservation is a main concern during active orthodontic treatment. A loss of anchorage results in a decrease of orthopedic force onto the maxilla. Therefore, new techniques have been developed to overcome the undesirable dental effects of conventional facemask therapy. These techniques include anchorage via mini-implants, onplants, and osseointegrated titanium implants[8].

Use of Conventional Facemask Therapy and Its Limitations

Conventional facemask therapy has been commonly used in treating patients who are skeletally class III. Ideally, patients will be overcorrected to compensate for the relapse that occurs. However, Ngan et al found that treatment of skeletal class III have a success rate of 50-60% at best[15]. If traditional facemask therapy is unsuccessful in bringing the maxilla forward, the patient may require orthognathic surgery to ultimately correct maxillary and mandibular jaw discrepancies. This procedure is performed after the patient has completed growing. For the patient, this incurs additional time and financial involvement along with the increased risk associated with the surgery. To improve upon traditional facemask therapy, we can understand how new techniques utilizing skeletal anchorage may be more beneficial in treating patients, allowing increased force to be applied to the maxilla.

In addition, timing of facemask therapy is critical due to its potential growth modification. Some studies have found that there is no statistical difference when treating patients who are younger (5-8 years) versus those who are older (9-12 years)[6,9]. However, others have found that with proper timing, class III malocclusions can be corrected via facemask therapy. To maximize skeletal effects and minimize dental effects, Delaire[16], McNamara[13], and Proffit[2] suggest that facemask therapy should begin before the age of 8. A

meta-analysis performed by Kim et al[17] found that facemask therapy is effective in patients that are growing, but the effects of the therapy were diminished in patients older than 9. This study showed that young patients had a mean A-point advancement of 0.9-2.9mm while older patients in late mixed dentition had minimal skeletal changes. Baccetti et al concluded that those in early mixed dentition had significant maxillary advancement with an upward and forward direction of condylar growth compared to those in late mixed dentition[18]. Another study by Melsona and Melson found that as age increased, the suture morphology became more interdigitated, making it more difficult to disarticulate the palatal bone from the pterygoid process[14].

Cha et al[15] showed that there were more dentoalveolar side-effects when facemask therapy was used in older patients. Patients who were post-puberty, demonstrated increased dentoalveolar effect (40%) with decreased skeletal effect (60%). This suggests that skeletal anchorage in patients above age 9 is indicated to maximize maxillary advancement while minimizing side-effects involving the dentition.

Maxillary Protraction with Skeletal Anchorage

In the past few years, research has been conducted to obtain varying modalities that can achieve skeletal anchorage such as the osseointegrated implants in the zygomatic buttress utilized by Singer et al[19]. These new treatment options improve upon traditional facemask therapy by redirecting forces skeletally while minimizing the dental effects of maxillary protraction.

One treatment modality that has been favored in recent studies is the placement of mini-plates for skeletal anchorage. Kircelli et al[20] studied midfacial protraction utilizing skeletally anchored mini-plates for maxillary advancement. There were a total of 6 subjects

with a mean age 11.8 years. He found that 2.8mm-8.6mm of maxillary protraction could be achieved. Despite the wide range that he obtained, his results showed that mini-plate anchorage had more maxillary advancement that conventional facemask therapy in patients of the same age.

Cevidanes et al[21] found that Bone Anchored Maxillary Protraction (BAMP) with class III elastics (Figure 2) had two to three millimeters more maxillary advancement than rapid maxillary expansion (RME) combined with facemask therapy. The mean age for the BAMP group was 11 years 10 months while the mean age of the RME/FM group was 8 years 3 months at the start of treatment.

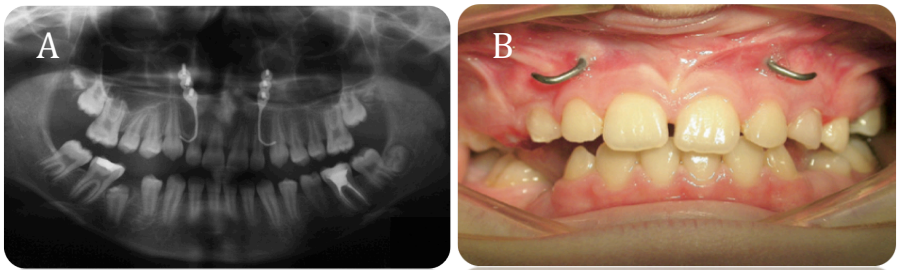

Figure 2. A. Panoramic film showing miniplates in the zygomatic buttress. B. Intraoral view of the mini-plates post-surgical placement.

A 2011 prospective, controlled, clinical study looked at treatment effects of facemask therapy with skeletal anchorage compared to conventional facemask[21]. They found that many of the unfavorable dentoalveolar effects of conventional facemask therapy were minimized or eliminated with miniplate anchorage.

Though these studies demonstrate that mini-plates are a promising method of maxillary advancement, a drawback to this method is the need for two surgeries. One surgery is needed for the placement of mini-plates and one is required for its removal. These

surgeries may be considered minimally invasive, but the increased time and risk associated with the procedures must be considered.

C. Circummaxillary Sutures

Another element critical to maxillary advancement is the anatomy of the skull. The sutures surrounding the maxilla act as soft tissue articulations between bones. Mao et al[22] states that sutures are important in absorbing and transmitting any mechanical stresses created in orthopedic loading. Therefore, suture biomechanics are important to consider when designing new methods of moving the maxilla.

Traditional facemask therapy alters growth at circummaxillary sutures by separating the sutures and translating the maxilla anteriorly. This requires 500-1500g of force and ideally the orthopedic force should be directly on these circummaxillary suture[23]. However, the displacement of the maxillary complex and zygomaticomaxillary suture can be altered by the direction of traction force[12,24]. As such, to obtain a more predictable amount of movement, the intraoral appliance design along with the direction of force is important to consider[25].

D. Finite Element Method (FEM)

Finite element method is a computer-aided numerical technique for finding approximate solutions to physical systems subjected to external influences under specific boundary conditions in order to solve complex problems in engineering, science and applied mathematics[26]. Originally developed by Courant to investigate torsion on a cylinder, its uses has now been expanded to analyze electromagnetic, thermal, fluid, and structural working environments[27]. The basic premise of FEM is that a large complex geometry can be

subdivided into simpler parts in order to accurately represent the complex geometry while including the dissimilar material properties and capturing the local effects[28].

Recently, the use of FEM has been incorporated into dentistry and orthodontics to study the nature of stress and strain induced by orthodontic forces during tooth movement[29]. More over, FEM has allowed the development of intricate craniofacial models in study the biomechanics involved with orthodontic forces on dental and facial structures[30,25]. Attributing to its abilities to break down complex geometries into simple geometric shapes with its unique material properties known as tetrahedron elements, FEM has allowed the analysis of stress and strain on intricate craniofacial models. Applying FEM to orthodontics, this powerful engineering tool has allowed the visualization of where craniofacial structures bend and twist while also revealing the distribution of displacements and stresses under different clinical loading conditions[26,28,29].

E. Image-based vs. CAD-based Mesh Generation

While complex finite element models of the head offer the prospect of creating accurate and reproducible clinical simulations on different orthodontic and orthopedic forces on the craniofacial complex, the validity of these models is largely influenced by the geometric accuracy of the structures within the model. In the past, computational models are generated manually using computer-aided design (CAD) tools. However, when interested in creating a 3D model that accurately preserves the complex anatomy of the head and its internal structures, this manual approach has substantial disadvantages. These disadvantages include the large scope of subjectivity of the user creating the model and in addition the computational difficulty as the fine geometric fidelity is added.

A novel model generation approach that can reduce the inaccuracies associated with the traditional CAD-based approach when modeling a highly complex structure is known as "image-based meshing". This type of innovative meshing technique involves the conversion of volume scan data, either from computed tomography (CT) or magnetic resonance imaging (MRI), directly into a finite element mesh via a fully and semi-automated processes with minimal user input. This innovative "image-based meshing" thus not only increases the accuracy of the model, but also the speed at which computational models of complex geometries such as the craniofacial complex can be constructed. This ultimately results in a more accurate preservation of the anatomical features of the original model of interest.

A prior investigation by Mehta et al. compared different imaging processing techniques including magnetic resonance imaging (MRI), computed tomography (CT) scan and ultrasound for 3-dimensional modeling and analysis of the human skull, tibia and fibula[31]. Mehta showed through 14 cross-sectional image 'slices' from an MRI scan of the head that these highlighted outlines of the bone can be selected using an image-processing tool and then read by C++ computer code and ultimately converted into computer-aided design CAD coordinate and spline data. With this process, Mehta was able to construct a model at least partially based on the true anatomy of the skull[31]. Since this early pioneering investigation done by Mehta et al., image-based modeling technology has improved tremendously. Presently, the generation of many sophisticated, geometrically accurate finite element model of the skulls rely in part to image-based meshing.

Developed by the US National Highway Traffic Safety Administration, the most up-to-date version of the Simulated Injury Monitor finite element head model (FEHM) is based on the CT data of the average male adult[32]. This finite element head model has been

validated against many experimental measures with its primary application for the measurement of injury potential of recorded head kinematic data using crash test dummies. This new image-based finite element head model provides the advantage over previous models due to the geometric preservation of the anatomic structures at the expense of additional computational time. In addition, in an investigation performed by Kraft et al. a complex image-based finite element head model was developed from T1-weighted MRI scan data[33]. This finite element model utilizes a diffusion tensor imaging (DTI) fiber tractography to accurate incorporate the structural orientation of neuronal axonal bundles in order to assess axonal strain during brain white matter deformation[34]. Furthermore, highly detailed, image-based finite element models have also been developed by various other groups including the University College Dublin Brain Trauma Model[35], the University of Salerno head model[36], and the University of Illinois head model[37].

The major limitation of these previous image-based finite element head models is the fact that they are provided as "fixed" and "immutable" finite element meshes. In other words, once the mesh is created, there is no means of making modifications to the mesh without having to create a completely new mesh model. Introduction of additional soft and hard tissues, or incorporation of additional components (orthodontic mini-implants, orthopedic mini-plates, etc.) is impossible without having to create a new mesh with these desired additions. As such, newly developed models will only work for specific problems and quickly become dated as improved imaging techniques open the possibility of more sophisticated and geometrically accurate models.

F. Aims of Study

The aims of the study are to:

- Using an image-based mesh generation approach, construct an anatomically accurate bone and circummaxillary suture density based FEM model of a complete skull from a patient with no craniofacial anomalies.
- From this anatomical mesh model, design simulations for different clinical protocols for maxillary protocols including conventional facemask therapy and micro-implant assisted rapid palatal expander (MARPE) facemask.
- Study and compare the skeletal effects, stress distributions, and displacements within the craniofacial complex when simulated protraction forces are applied to the maxilla.
- Compare the results from the newly generated image-based mesh model to the previous CAD-based mesh model.
- Correlate the simulated findings to how clinical protocols can be improved and modified in treatment of growing class III individuals.

G. Hypothesis

- The newly generated image-based finite element head model will provide more accurate clinical simulations of orthopedic and orthodontic tooth movements compared to the previous computer-aided design (CAD) based mesh model.
- In comparison between the conventional facemask therapy and with the use of micro-implant assisted rapid palatal expander (MARPE), the MARPE with

facemask will produce less dental side-effects and provide better maxillary protraction.

Materials and Methods

A. Computed Tomography (CT) Raw Data

Medical spiral CT scan of a 42-year-old male patient with informed consent was obtained from the Department of Biomedical Sciences at Ohio University. Due to is comparably intrinsic high-contrast resolution, spiral CT was chosen over the standard 3D radiography utilized in orthodontics, the Cone-Beam CT (CBCT), for obtaining the DICOM raw data. The spiral CT inherently allows more clearly defined hard-tissue boundaries for creation of highly accurate 3D finite element mesh models that would not have been possible using the conventional CBCT[38].

The CT scan used in this study was executed with the following specifications: 120 kV, 360 mA, 512x512 matrix size, 0.300 mm slice thickness, and 0.463 x 0.463 x 0.300 voxel size. Further modifications were performed on the CT image date to remove foreign artifacts, scatter and the pre-existing mandible from the 3D skull model.

B. Finite Element Analysis

Finite element analysis is traditionally separated into three different components:

1) Pre-processing

2) Solution

3) Post-processing

C. Pre-processing Stage

In this first stage of finite element analysis, the raw DICOM data from the spiral CT of the patient is converted into the 3D FEM mesh model. The FEM model is generated first by importing the CT volumetric data into Simpleware +FE Module 7.0 software from Exeter, United Kingdom (Figure 3).

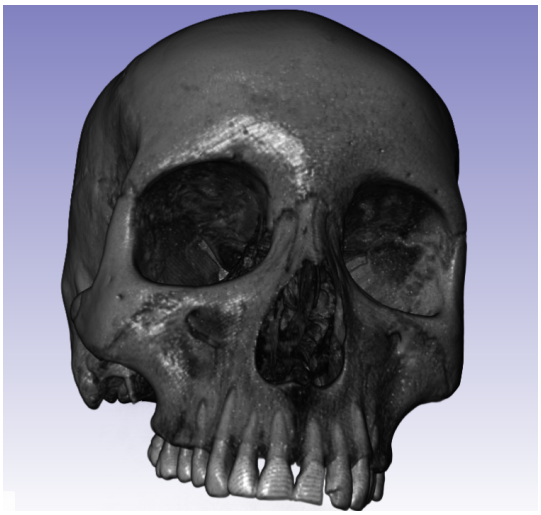

Figure 3. 3D Skull Generation

Similar to the image-based mesh generation approach presented by Young et al, different masks are created for the different region of interests including the bone and the various circummaxillary sutures: mid-palatal, pterygomaxillary (2), zygomaticomaxillary (2), zygomaticotemporal (2), lateral nasal (2) and median nasal[39] (Figure 5). Each of these masks is defined based on the image grayscale within the region of interest. The different voxels from these masks are then converted directly into finite elements based off a technique called Extended Volumetric Marching Cubes (EVOMAC) approach used in the Young study. The previous mesh model used by orthodontic residents at UCLA utilized the traditional CAD-based mesh generation approach using the Mimics software and required manual placement

of these sutures (Figure 4). This more traditional CAD based approach is subject to user bias and many inaccuracies as the position of the sutures are subjective and do not rely on the patient's actual anatomy.

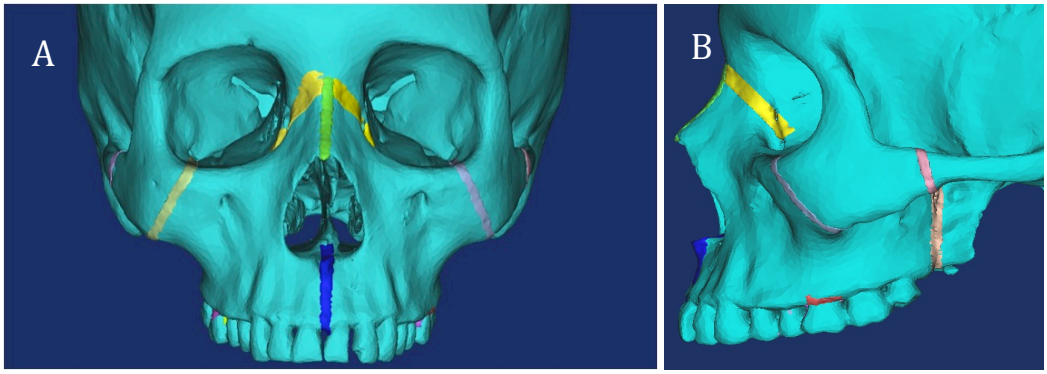

Figure 4. 3D skull with manually generated sutures. A. Frontal View B. Lateral View

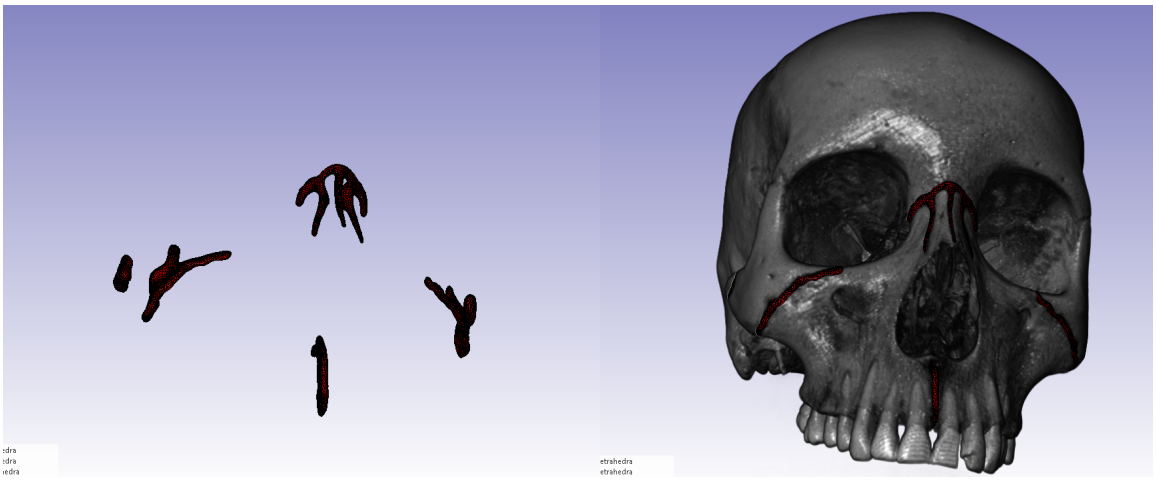

Figure 5. Circummaxillary sutural mesh extracted from DICOM data.

In addition, the previous CAD-based finite element model required many steps in order to clean up the model such as the use of Laplacian boundary-edge function, triangular reduction and remeshing. These additional processes are time-consuming and were used to remove the sharp edges in the model and to remove any overlapping and misshapen triangles. Furthermore, this previous CAD-based mesh model utilized a 4-node linear tetrahedral structural solid (figure 6) known as SOLID72 as the unit element for the 3D mesh. While four-node linear elements are computationally easier to compute, they are less accurate in displacement based finite element analysis compared to the more expensive 10-node quadratic tetrahedral element known as SOLID187 used in the generation of this new mesh (Figure 7). While the SOLID72 consisted of four nodes each with six degrees of freedom, including translation and rotation in the x, y and z directions, the most advanced SOLID187 has a quadratic displacement behavior and is a higher order 3-D, 10-node element that has three degrees of freedom at each node, including translation in the x, y, and z directions[40,41].

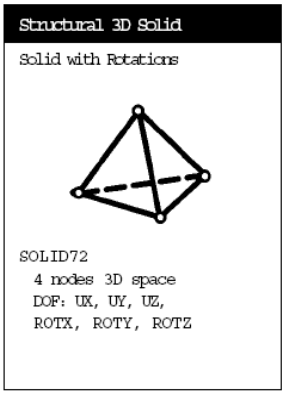

Figure 6. 3D 4-Node Tetrahedral Structural Solid (SOLID72)

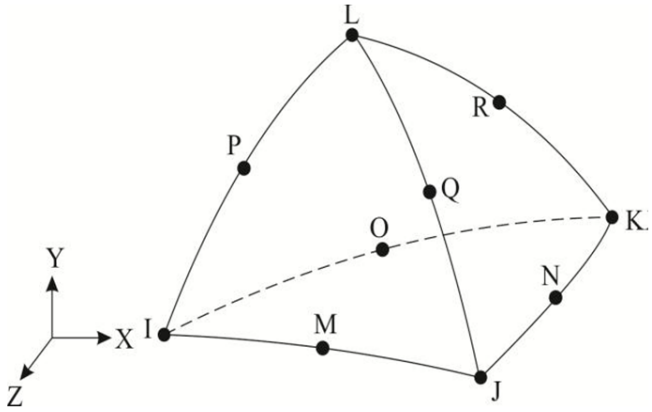

Figure 7. 3D 10-Node Tetrahedral Structural Solid (SOLID187)

In the previous CAD-based finite element mesh model, material properties of the skull and craniofacial sutures were assigned to elements via ANSYS. The bone and tooth structure in the model was assigned properties of compact bone: Poisson's ratio of $\nu = 0.3$ and a Young's Modulus of $E = 1.37 \times 10^3$ (kg/mm^2)[23,42]. Sutural elements were assigned values of connective tissue: $\nu = 0.49$ and $E = 6.8 \times 10^{-2}$ (kg/mm^2)[23,42–44].

In the new image-based finite element mesh model, Hounsfield (HU) units from the spiral CT was extracted from the DICOM data and converted into different density material properties. The threshold segmentation function within Simpleware +FE software analyzes the tissue density of each CT slice in Hounsfield Units (HU). Generally, Hounsfield units is a scale of relative densities based on air (-1000), water (0), and dense bone (+1000)[26]. +FE software was utilized to distinguish HU values between 0 and 1950 to identify the hard tissues of interest, including enamel, cancellous bone, compact bone and circummaxillary sutures resulting in a 3D mask of the craniofacial complex. Since the enamel within the DICOM data produced grayscale values from 2000-4000, an upper limit of 1950 grayscale

value was applied to represent the densest areas of the bone (Figure 8). A linear relationship was then used to determine the density of the materials from the HU values of the DICOM data using the following equation: rho = a + b*GS; and the following mapping function from mass density to Young's modulus in the form E=a+b*(rho)^c [45].

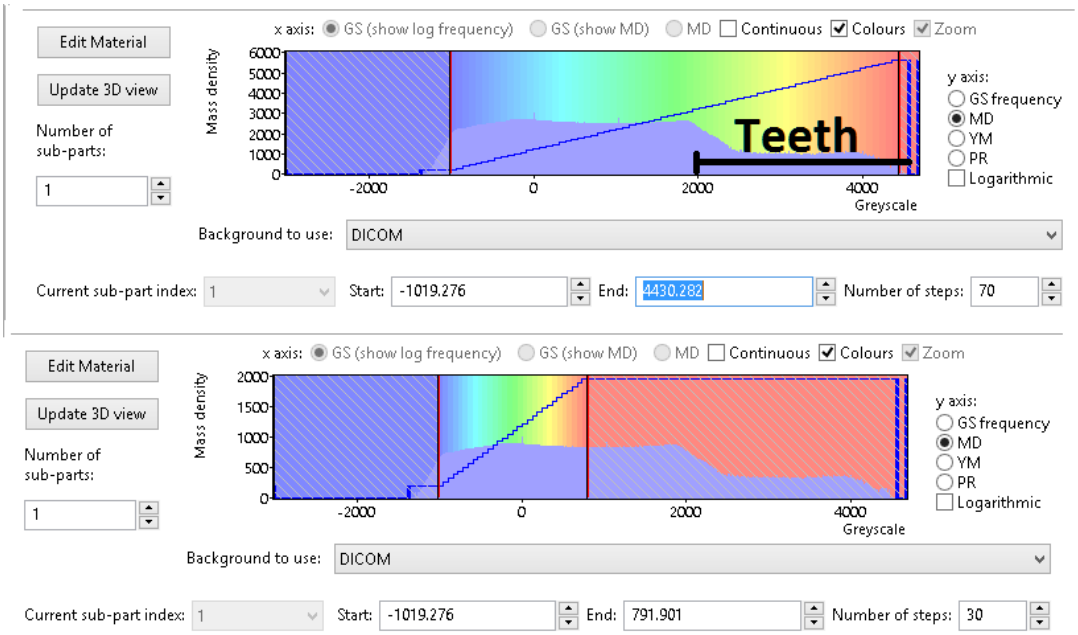

Figure 8. Histogram of Grayscales

Previous FEM mesh models used by previous orthodontic residents consisted of 91,933 nodes and 344,451 elements. As the goal of this study was to increase the resolution and anatomical accuracy of the mesh model, the element count was first increased from 344,451 elements to 1 million elements. Due to the detail around the sutures and maxilla region of the face, the mesh towards the back of the skull became quite coarse and resulted in regions that have 1-2 elements across. Since the grayscale mapping assigns a density value to each element of the mesh based on the average grayscale in that element, the area of lower density between the high-density outer and inner layers of the skull is not accurately

captured. As such, the resulting mesh was increased from 1 million to 2.4 million elements to accurately show the differences in density values (Figure 9).

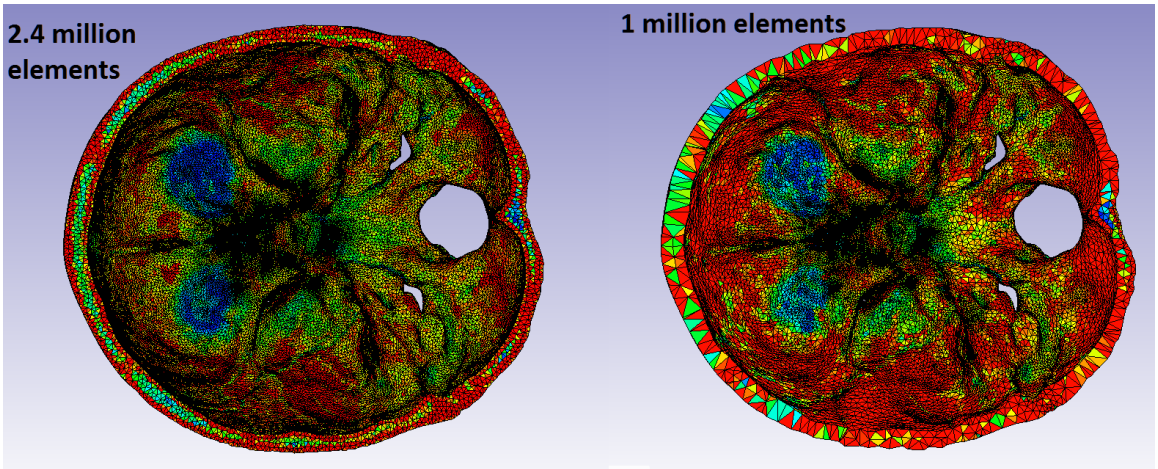

Figure 9. Density Mapping Comparison between 2.4 Million vs. 1 Million Elements

Due to the original DICOM data being from a 42 year-old male patient, the patency of the mid-palatal suture was not present (Figures 10A and 10B). However, we were able to extend the mid palatal suture with a traditional CAD-based approach in order to evaluate clinical simulations of patients with patent mid-palatal sutures (Figure 11A and 11B).

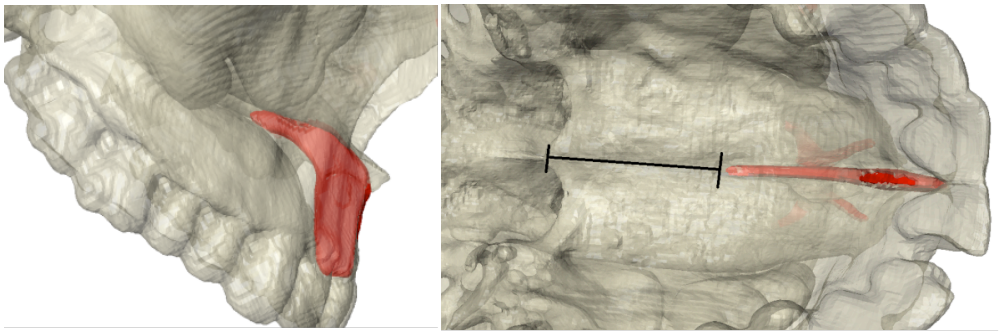

Figure 10A and 10B. Mesh of Mid-Palatal Suture Based off of Image Grayscale

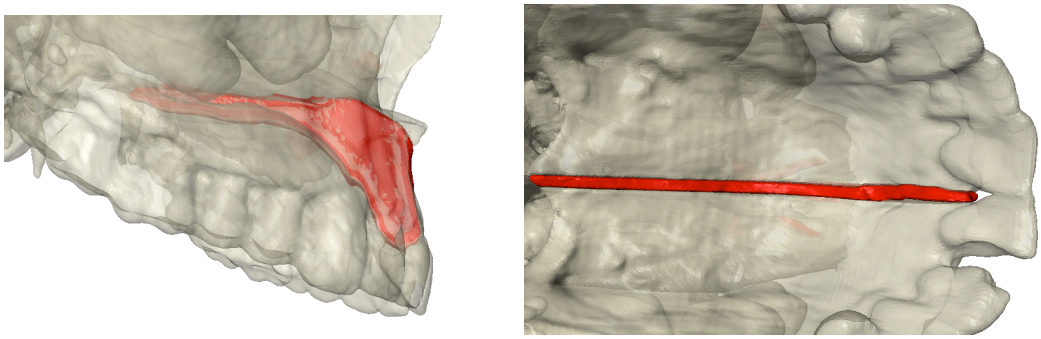

Figure 11A and 11B. Extended Mesh of Mid-Palatal Suture

Finally, the 3D mesh from Simpleware was imported into ANSYS 15.0 (ANSYS Inc., Canonsburg, PA) FEM software program (Figure 12).

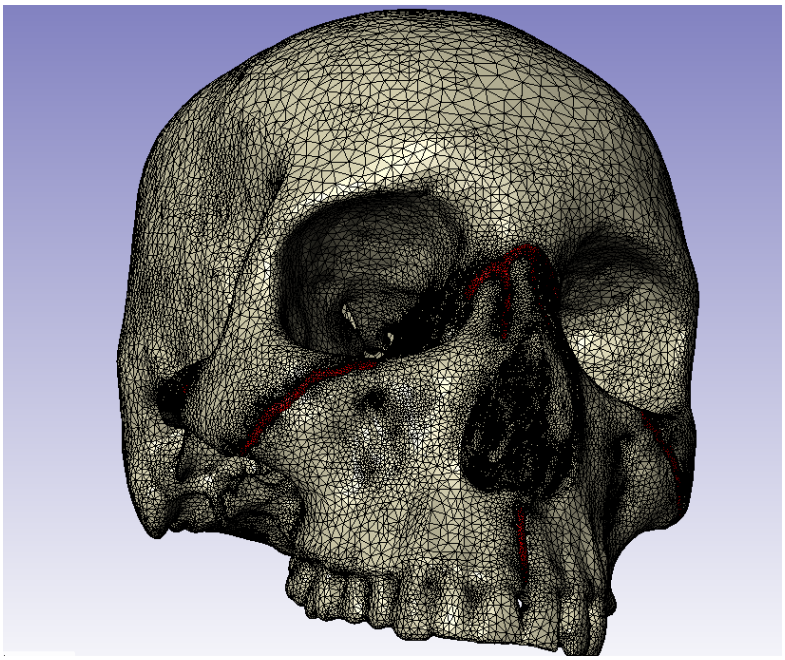

Figure 12. Combined 3D mesh of craniofacial bones and sutures.

D. Solution Stage

The solution stage of finite element analysis involves determination of boundary conditions and force application.

Boundary Conditions: Nodes along the foramen magnum and on the center of the forehead were constrained in all degrees of freedom, with zero displacement and zero rotation (Figure 13) [25].

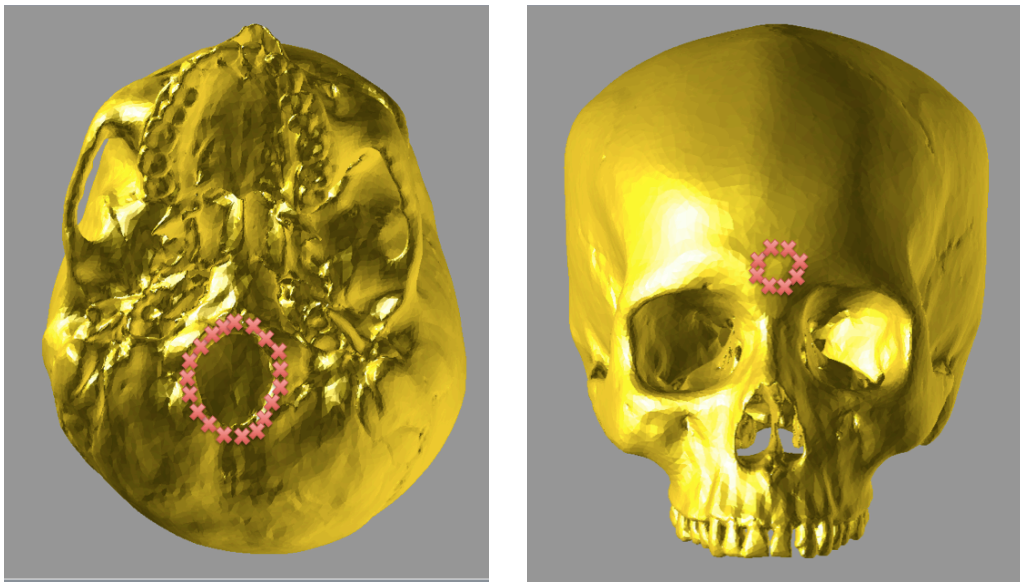

Figure 13. Red "X" depicts where nodes along the foramen magnum and on the center of the forehead are constrained.

Force Loading: Different locations and directions of force application were applied to simulate two different clinical protocols for maxillary protraction. Simulation A simulates conventional facemask therapy, where a 1000-gram force is applied to the buccal surface of the first maxillary molars, angled 30° below the occlusal plane (Figure 14). Simulation B simulates use of micro-implant assisted rapid palatal expander (MARPE) with the use of

facemask and is the same protocol used in the UCLA clinic (Figure 15). In this protocol, bilateral 1000-gram forces are applied 3mm lateral to the mid-palatal suture, at a 30° angle below the occlusal plane.

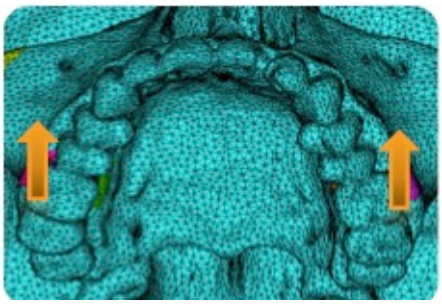

Figure 14. Location of force application for Simulation A - FM (-30°)

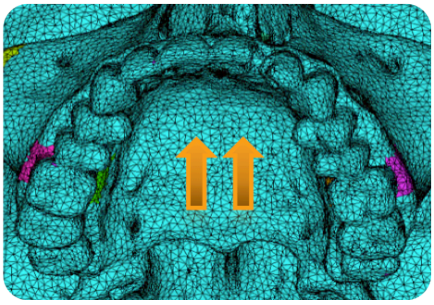

Figure 15. Location of force application for Simulation B - MARPE-FM (-30°)

E. Post-processing Stage

With the ANSYS software:

1. Contour plots from the nodal and element solutions were plotted to reveal areas of high stress and displacement. First principle and third principle stresses were used to measure the tensile and compressive stresses for both simulations.

2. Video animations were generated for both simulations.
3. 3D superimpositions were generated to show the skeletal displacement as a result of force loading.

Calculation of Principle Stresses:

$$\boldsymbol{\sigma} = \begin{bmatrix} \sigma_{11} & \sigma_{12} & \sigma_{13} \\ \sigma_{21} & \sigma_{22} & \sigma_{23} \\ \sigma_{31} & \sigma_{32} & \sigma_{33} \end{bmatrix} \equiv \begin{bmatrix} \sigma_{xx} & \sigma_{xy} & \sigma_{xz} \\ \sigma_{yx} & \sigma_{yy} & \sigma_{yz} \\ \sigma_{zx} & \sigma_{zy} & \sigma_{zz} \end{bmatrix} \equiv \begin{bmatrix} \sigma_x & \tau_{xy} & \tau_{xz} \\ \tau_{yx} & \sigma_y & \tau_{yz} \\ \tau_{zx} & \tau_{zy} & \sigma_z \end{bmatrix}$$

Using the above cubic equation, all principle stresses within each node in the model was calculated. The most positive root after the determinant is expanded is defined as σ1, which represents first principle stress and also correlates with the tensile stresses. The most negative value is defined as σ3 representing third principle stresses and correlates with compressive stresses. The second principle stress commonly approaches zero, and therefore is not significant for this study.

Results

Model Generation:

The new image-based FEM model generated with Simpleware yielded 3,790,867 nodes and 2,376,848 elements. However, due to the limitations with the hardware memory, the elements and nodes were reduced to 1,597,012 nodes and 1,018,142 elements. With this reduced model, a greater concentration of elements were designed around the circummaxillary complex of the skull and thus larger elements were placed in the posterior cranium which is furthest from the location of force application.

Model Comparison:

A. First Principle Stresses

Figures 16-22 illustrate the distribution of first principle stresses correlating to tensile stresses in Simulation A and B, in the frontal, occlusal, and lateral views respectively.

Figure 16: Scale for 1st Principle Stresses

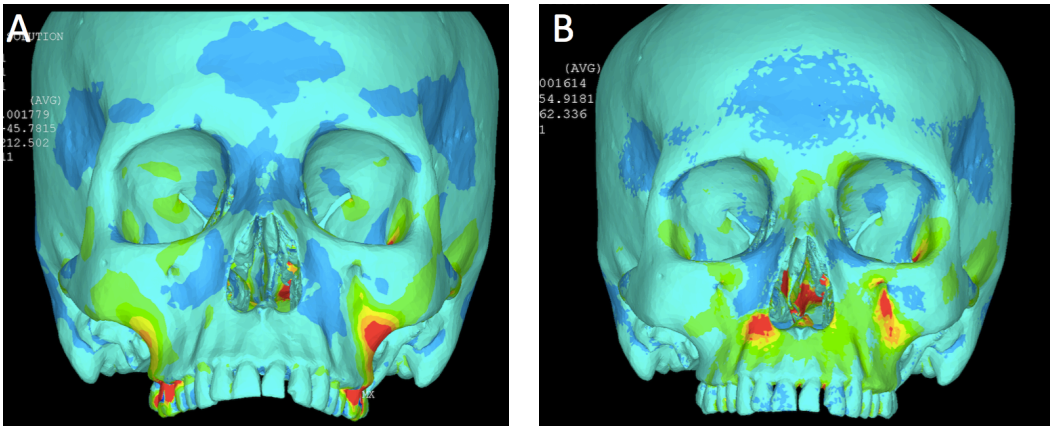

Figure 17: Frontal View of 1st Principle Stresses from New Image-Based Model.

A: Conventional FM [-30°] B: MARPE-FM [-30°]

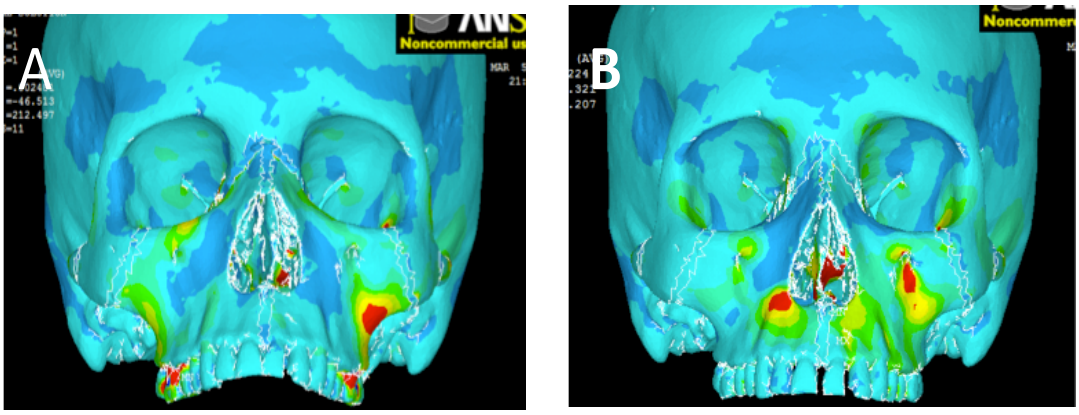

Figure 18: Frontal View of 1st Principle Stresses from Previous CAD-Based Model.

A: Conventional FM [-30°] B: MARPE-FM [-30°]

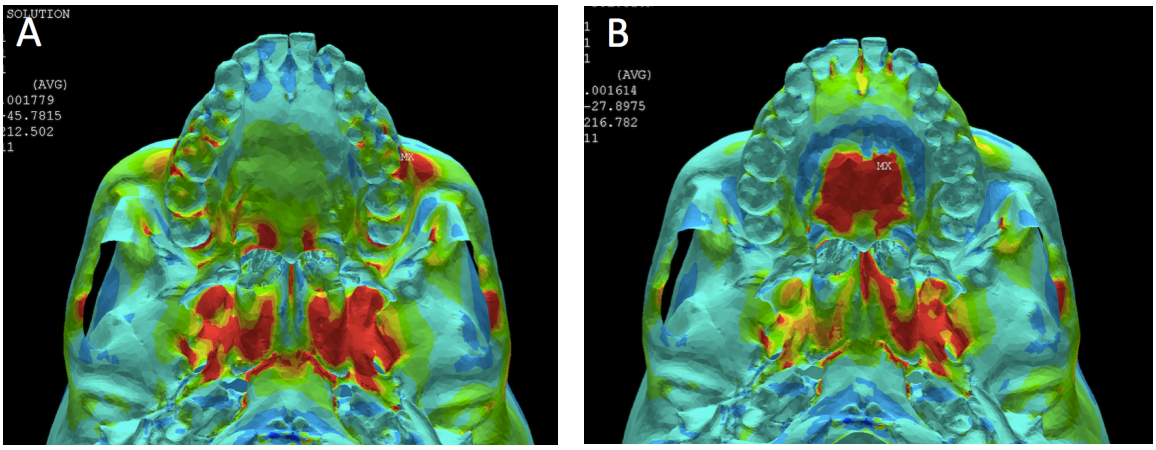

Figure 19: Occlusal View of 1st Principle Stresses from New Image-Based Model.

A: Conventional FM [-30°] B: MARPE-FM [-30°]

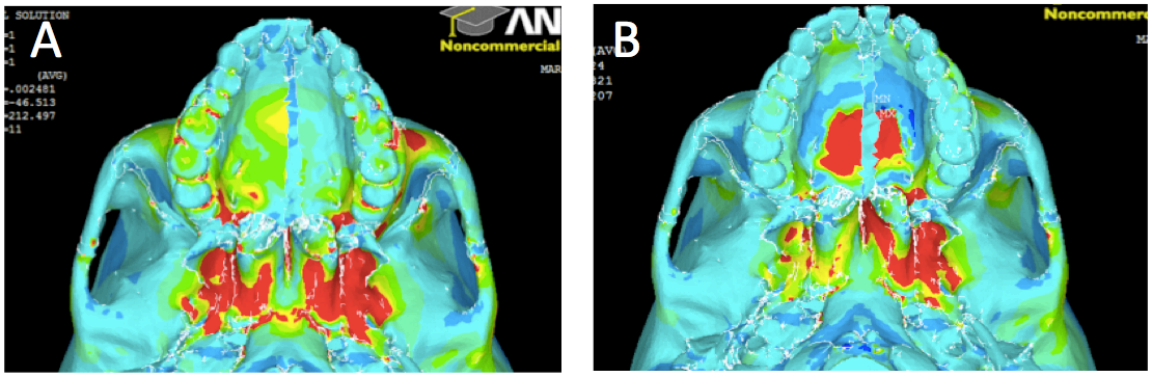

Figure 20: Occlusal View of 1st Principle Stresses from Previous CAD-Based Model.

A: Conventional FM [-30°] B: MARPE-FM [-30°]

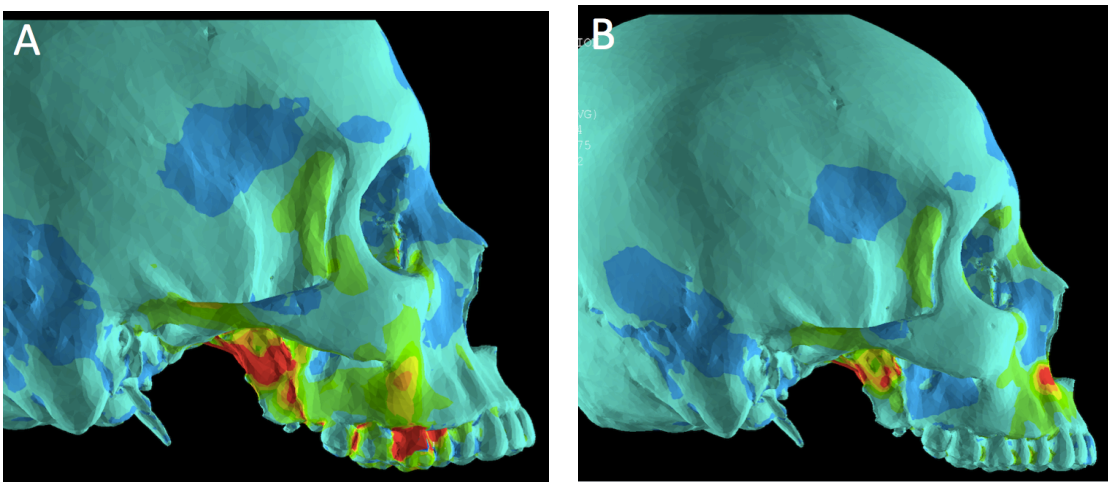

Figure 21: Lateral View of 1st Principle Stresses from New Image-Based Model.

A: Conventional FM [-30°] B: MARPE-FM [-30°]

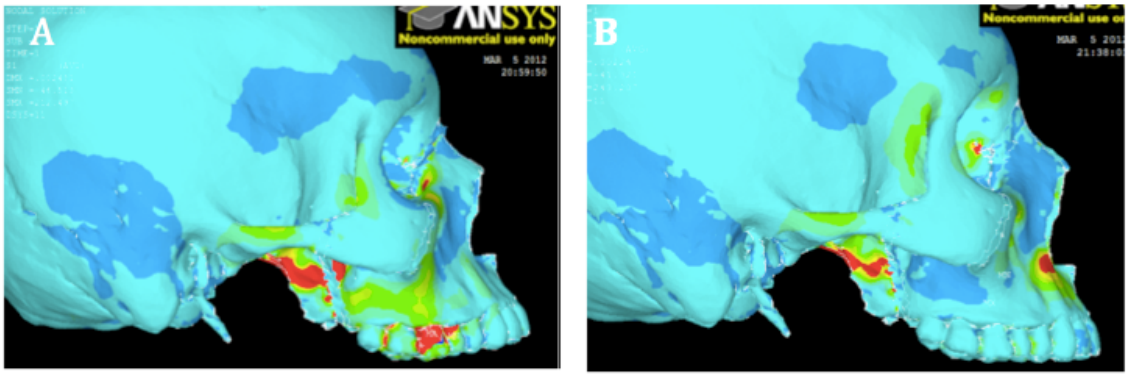

Figure 22: Lateral View of 1st Principle Stresses from Previous CAD-Based Model.

A: Conventional FM [-30°] B: MARPE-FM [-30°]

For all of the simulations, there is a high concentration of tensile stress directly posterior to the location of force application. Furthermore, tensile stresses also concentrated at the pterygoid plates in all simulations with slightly more stress overall with the new image-based model. In Simulation A, in both the old CAD-based model and the new image-based model, this stress encompasses the maxillary first molar. In Simulation B, high levels of tensile stress are located in the posterior portion of the palate, but not involving the mid-palatal suture in the previous CAD-based model. However, this tensile stress was present and evenly distributed through the midpalatal suture bilaterally with the use of the new image-based model. Finally, tensile stresses are congregated near the maxillary buttress in simulation A with the image-based model showing slightly increased amounts.

B. Third Principle Stresses

Figures 23-29 illustrate the distribution of third principle stresses correlating to compressive stresses in Simulation A and B, in the frontal, occlusal, and lateral views respectively.

Figure 23: Scale for 3rd Principle Stresses

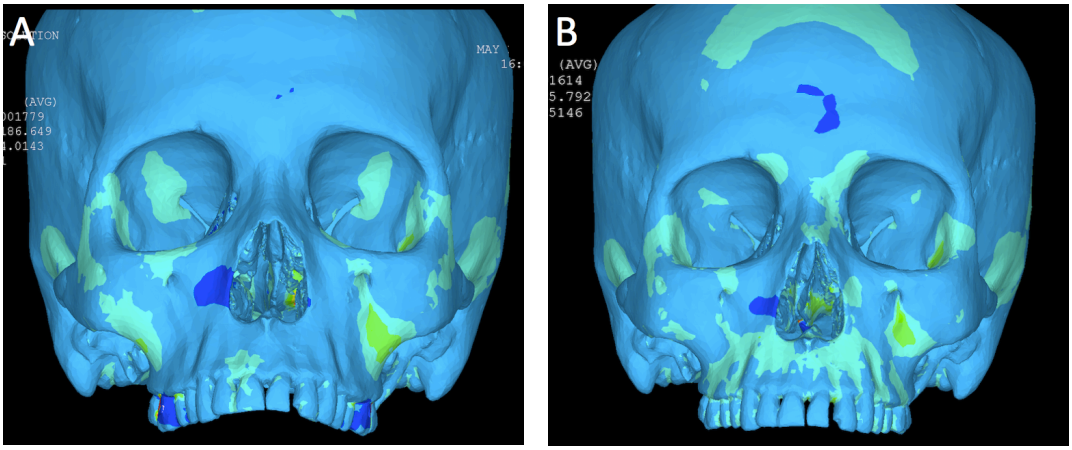

Figure 24: Frontal View of 3rd Principle Stresses from New Image-Based Model.

A: Conventional FM [-30°] B: MARPE-FM [-30°]

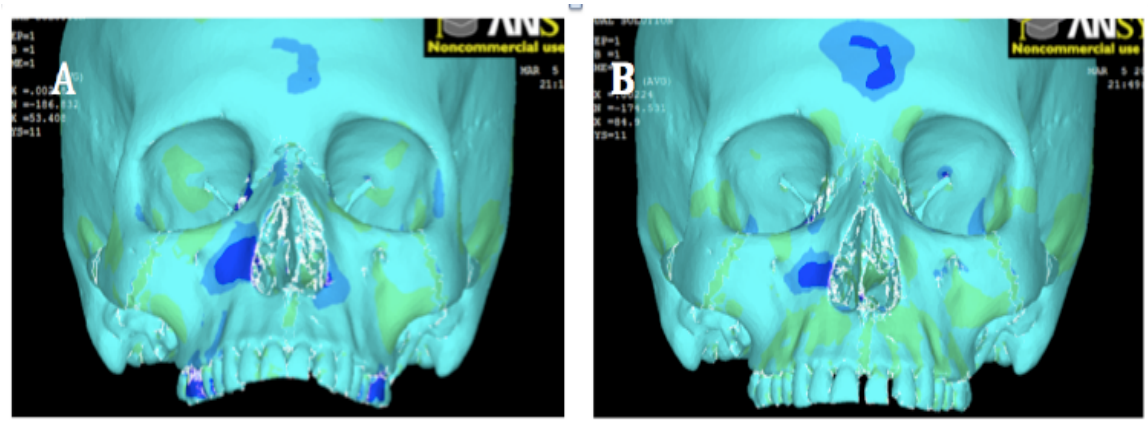

Figure 25: Frontal View of 3rd Principle Stresses from Previous CAD-Based Model.

A: Conventional FM [-30°] B: MARPE-FM [-30°]

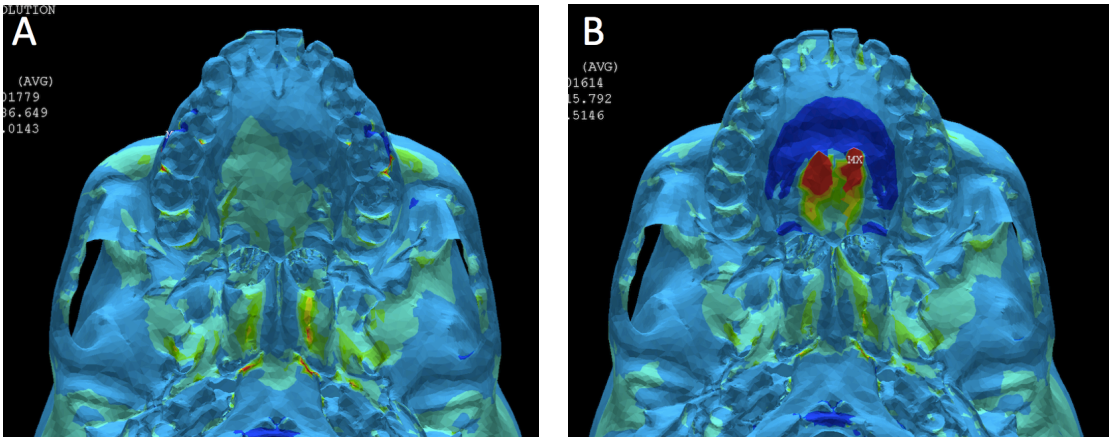

Figure 26: Occlusal View of 3rd Principle Stresses from New Image-Based Model.

A: Conventional FM [-30°] B: MARPE-FM [-30°]

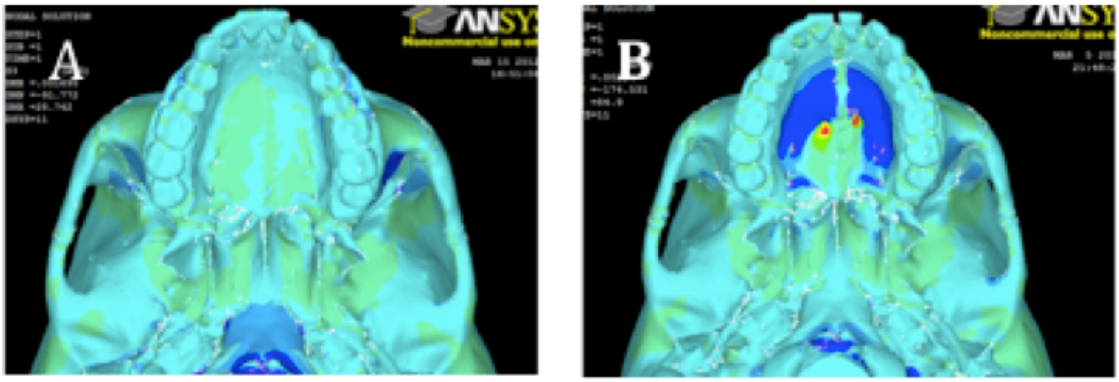

Figure 27: Occlusal View of 3rd Principle Stresses from Previous CAD-based Model.

A: Conventional FM [-30°] B: MARPE-FM [-30°]

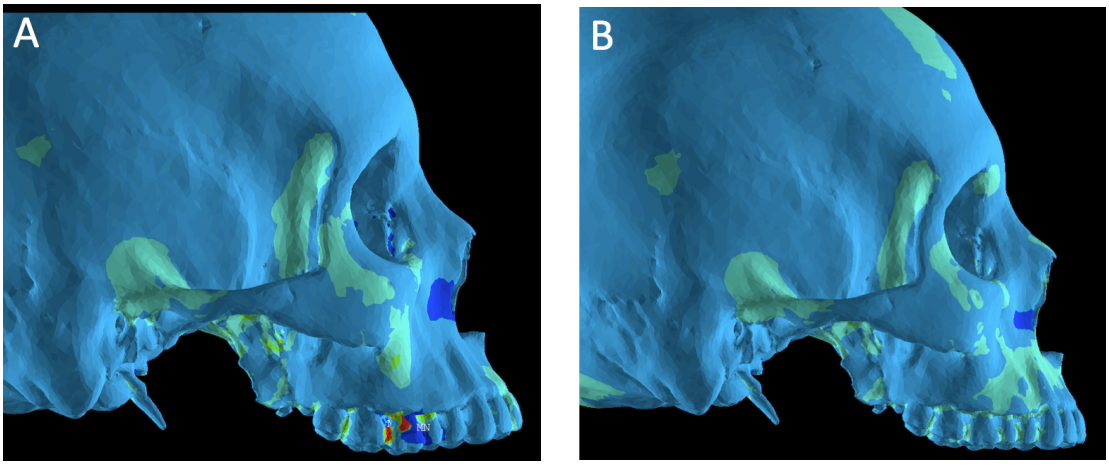

Figure 28: Lateral View of 3rd Principle Stresses from New Image-Based Model.

A: Conventional FM [-30°] B: MARPE-FM [-30°]

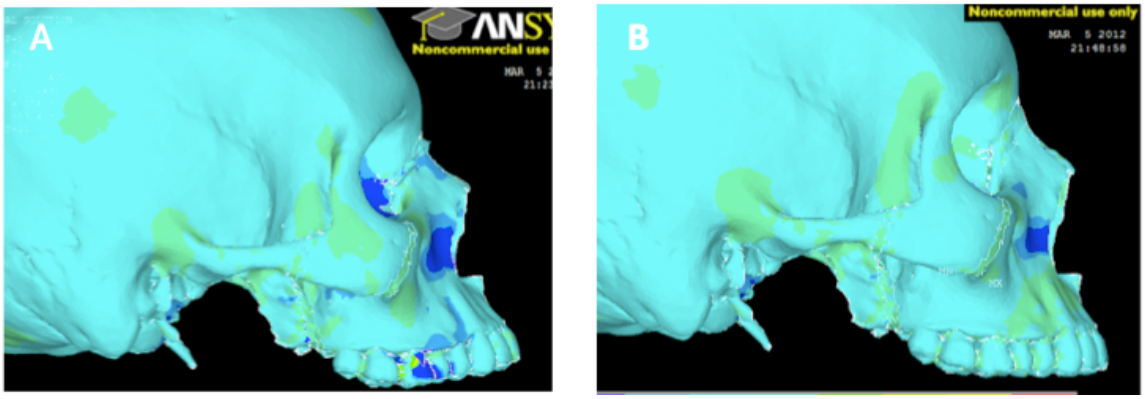

Figure 29: Lateral View of 3rd Principle Stresses from Previous CAD-Based Model.

A: Conventional FM [-30°] B: MARPE-FM [-30°]

For all of the simulations, there is a high concentration of compressive stress directly anterior to the location of force application. In addition, all simulations regardless of the model type displayed compressive stresses in the forehead area. In Simulation A, compressive stress congregates around the mesial region of the maxillary first molar similarly for both the previous CAD-based model and the new image-based model. For Simulation B, high compressive stresses can be seen in the anterior and lateral portion of the palatal. This

compressive force does not involve the mid-palatal suture for the previous CAD-based model and does involve the mid-palatal suture for the new image-based model.

C. Displacement (via Superimpositions)

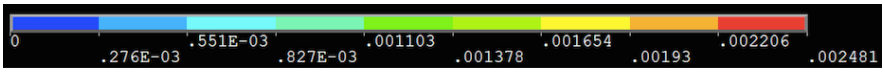

Figure 30: Scale for Displacement

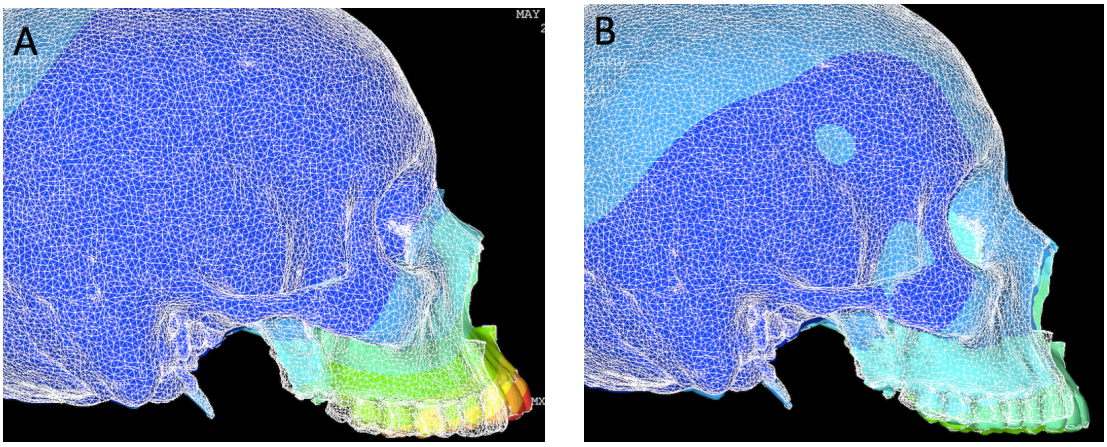

Figure 31: Displacement along Y-axis (sagittal) Superimposed on "Un-deformed" Previous CAD-Based Model

A: Conventional FM [-30°] B: MARPE-FM [-30°]

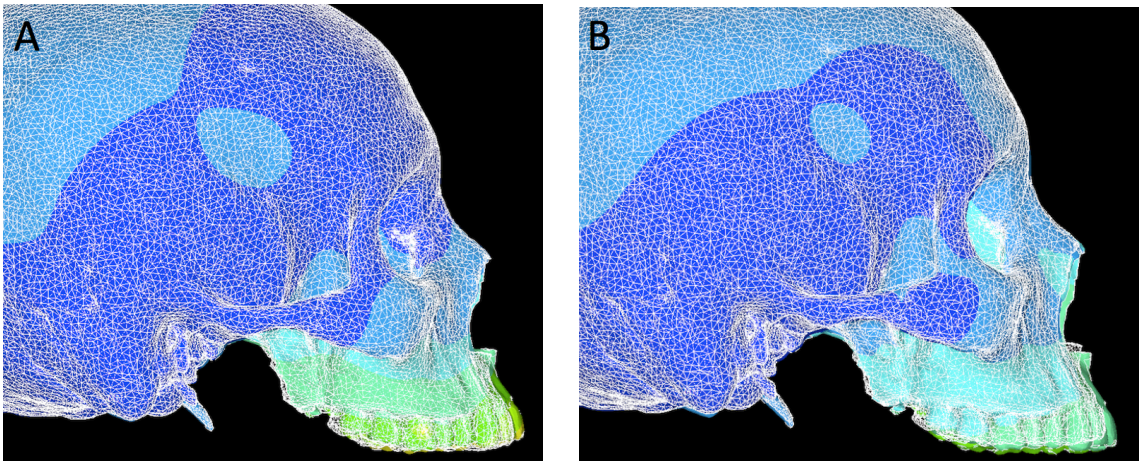

Figure 32: Displacement along Y-axis (sagittal) Superimposed on "Un-deformed" New Image-Based Model

A: Conventional FM [-30°] B: MARPE-FM [-30°]

When superimposing the previous CAD-based model with its original "un-deformed" model, Simulation A showed significant anterior tipping of the maxilla in a counter clock-wise direction while Simulation B showed significant downward and forward translational movement of the maxilla. When superimposing the new image-based model with its original "un-deformed" model, Simulation A showed slightly less anterior tipping of the maxilla in a counter clock-wise direction while Simulation B showed slightly less downward and forward translational movement of the maxilla.

D. Video Animations

Animation videos of each simulation were created. All videos have been included in the supplemental section named Simulations A-B for both the previous CAD-based model

and the new image-based model. The table below summarizes the general and significant findings from each simulation video (Figure 33).

Model	Simulation	Clinical Protocol	Movement of maxillary complex	Other Significant Findings
CAD-Based	A	FM [-30°]	Counter-clockwise Rotation	Dentoalveolus is protracted forward and upward
CAD-Based	B	MARPE-FM [-30°]	Translates forward and downward	Maxillary complex translates downward and forward
Image-Based	A	FM [-30°]	Counter-clockwise Rotation	Dentoalveolus is protracted forward and upward
Image-Based	B	MARPE-FM [-30°]	Translates forward and downward	Maxillary complex translates downward and forward

Figure 33. Summary of maxillary movement following force application.

Discussion

A. Simulations & Clinical Applications

For all Simulations, 1000g of protraction forces were applied, as many investigations have demonstrated that a force load between 500-1500g is ideal for maxillary protraction. After running Simulation A and Simulation B with the newly developed image-based model, similar tensile stresses were visible posterior to the site and direction of the force loading, while similar compressive stresses were seen anteriorly. The magnitude of the tensile and compressive stresses however, were slightly larger than the same simulations conducted on the previous CAD-based model.

Furthermore, the video animations and the superimpositions help to validate the accuracy of the new image-based model. The center of resistance (CR) of the maxilla is designated by the ⊕ symbol in both the lateral and frontal views of figure 34. From the lateral view, the center of resistance of the maxilla is located along a vertical line tangent to

the distal of the maxillary first molar and then selected by bisecting the distance from the functional plane to the inferior border of the orbit[46]. From a frontal view, the center of resistance of the maxilla is derived from the perpendicular intersection of an axis through crista galli and through the most inferior part of the zygomaticomaxillary sutures bilaterally (Figure 34).

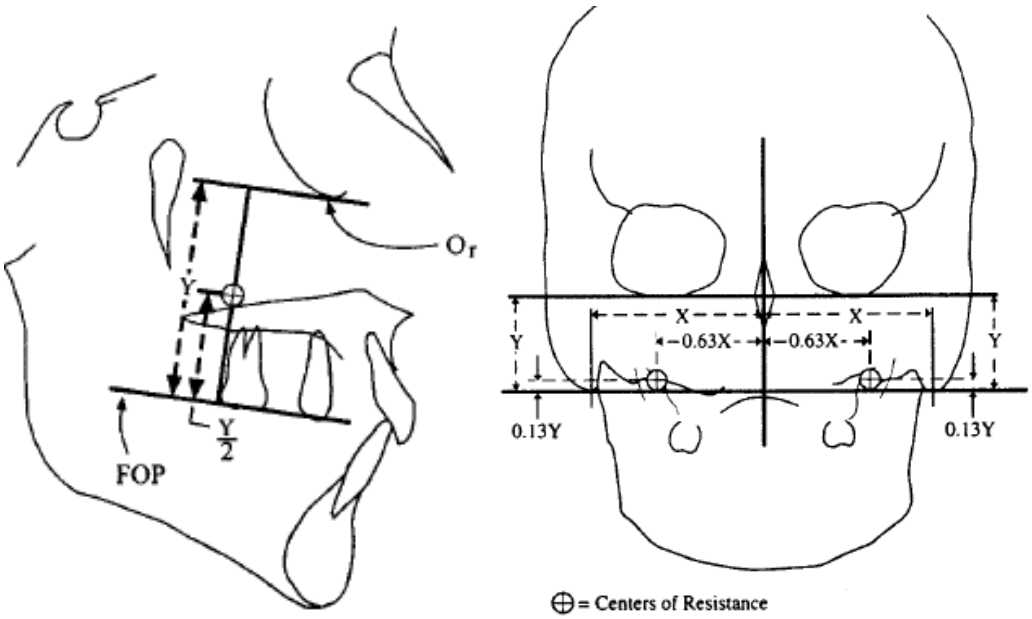

Figure 34. Center of Resistance of the Maxilla

The most important aspect of validating the new image-based model requires the understanding of the center of resistance from the lateral view. When protraction forces are applied below the center of resistance of the maxilla, it has been proven that the maxillary complex will rotate in a counter-clockwise direction. This is accurately seen in the displacement superimpositions and in the video animations of Simulation A in both the old CAD-based model and the new image-based model. However, Simulation A in the old CAD-based model produced displacements that are quite exaggerated and resulted in

significant anterior tipping of the maxilla. This type of maxillary movement is not biologically possible as the maxilla cannot physically impact itself without some type of surgical intervention. As such, Simulation A based off of the new image-based mesh demonstrates a more realistic type of maxillary movement that would be expected when a force is applied below the center of resistance of the maxilla.

When protraction forces are applied through the center of resistance of the maxilla, it has been proven that the maxillary complex will translate in a downward and forward direction. This is accurately seen in the displacement superimpositions and in the video animations of Simulation B in both the old CAD-based model and the new image-based model. However, Simulation B in the old CAD-based model produced displacements that are quite exaggerated and resulted in significant downward and forward translation of the maxilla without any rotation. While not impossible, this type of maxillary movement is most likely overstated due to the simplification of the bone and suture material properties. As such, Simulation B based off of the new image-based mesh demonstrates a more realistic type of maxillary movement that would be expected when a force is applied through the center of resistance of the maxilla.

While the displacement superimpositions and the video animations are valuable for demonstrating the skeletal response of the force loading, they cannot accurately predict the dental response since the PDL has not been incorporated into the mesh. Studies have shown that PDL ranges from 0.5-1mm in width and due to the memory constraints of the computer and element size, the PDL is not meshed in the model[43]. As such, the teeth in these models are essentially ankylosed to the dentoalveolar bone. Simulation A in both the previous CAD-based model and the new image-based model do not have the ability to accurately show the

extrusion, buccal tipping, mesial movement of the maxillary molars and proclination of the maxillary incisors are seen in conventional facemask therapy[7,18,47]. However, the skeletal effects of this simulation shows that this maxillary protraction protocol may be useful for class III brachyfacial patients with a deep overbite and short lower facial height as this would effectively open the bite and increase the lower facial height.

Examining Simulation B, the use of micro-implant assisted rapid palatal expander with a facemask reveals that the maxillary complex translates downward and forward equally. This is similar to the clinical effects of a LeFort 3 advancement as the entire midfacial segment has been translated downward and forward[16,48]. As such, this protocol can be used in mild class III patients with a shallow bite.

B. Study Limitations

The finite element model was based off a CT scan of a 42-year-old male patient. As such, the actual sutural morphology and bone densities will vary greatly from that of a growing patient. While the general shape of the model is that of an adult, the sutures were modified to be more representative of an adolescent.

Two different image-based finite element meshes were generated. The first image-based mesh contained the optimal number of elements and nodes for the most precise representation of the original CT scan of the patient. This model contained 2,376,848 elements and 3,790,867 nodes. However, due to the utilization of the most advanced 10-node SOLID187 elements, this model was computationally expensive to the point where simulations were taking more than 20 days to perform. As such, a second image-based finite element model with 1,018,142 elements and 1,597,012 nodes was generated. This model

contained coarser elements in the posterior cranium and thus the material density of the posterior skull was less accurate than the original 2.4 million model.

Due to this limitation in computer processing, the PDL of the teeth were also not incorporated into the model. As such, the newly generated model has teeth that are essentially ankylosed to the skull. The mesh model also does not include bone remodeling or biological osteoblastic or osteoclastic activity. This greatly inhibits the accurate prediction of dental movement with different clinical simulations. Also, the mesh model does not include the mandible or any soft tissue or muscular attachments.

Further refinement or introduction of the PDL, soft tissues and biological remodeling of the bone may provide even more accurate depiction of clinical simulations for future studies. With the development of faster and more powerful computers, the newly developed model with 2.4 million elements can be used to provide even more accurate clinical simulations.

Conclusions

In the past, early treatment of class III skeletal malocclusions has been attempted with facemask therapy, which has been shown to be effective in younger growing patients. However, many dental side-effects and less skeletal improvement can be seen after age 9. Skeletal anchorage achieved with the placement of mini-plates has demonstrated predictability in the protraction of the maxilla even in non-growing patients. However, the use of mini-plates requires the surgical placement and removal of the mini-plates. In this study, an image-based mesh model was created with anatomically accurate location and material properties of the bone and sutures to better predict two different types of maxillary

protraction protocols in hopes of providing improved skeletal anchorage without the use of mini-plates.

The displacement superimpositions and video animations showed that the new image-based mesh model has improved clinical predictability when compared with the previous CAD-based mesh model. Finally, the skeletal response from two different clinical simulations showed that these two different protocols can be applied to different types of patients to maximize the desired skeletal effects.

References

1. Chang, H. P., Kinoshita, Z. & Kawamoto, T. Craniofacial pattern of Class III deciduous dentition. *Angle Orthod.* **62,** 139–144 (1992).

2. Proffit, W. R., Fields, H. W. & Sarver, D. M. *Contemporary orthodontics*. (Mosby Elsevier, 2007).

3. Hägg, U., Tse, A., Bendeus, M. & Rabie, A. B. M. Long-term follow-up of early treatment with reverse headgear. *Eur. J. Orthod.* **25,** 95–102 (2003).

4. Ellis, E. & McNamara, J. A. Components of adult Class III malocclusion. *J. Oral Maxillofac. Surg. Off. J. Am. Assoc. Oral Maxillofac. Surg.* **42,** 295–305 (1984).

5. *Orthodontic Treatment of Class III Malocclusion*. (BENTHAM SCIENCE PUBLISHERS, 2014). at <http://www.eurekaselect.com/123372/volume/1>

6. Ngan, P. W., Hagg, U., Yiu, C. & Wei, S. H. Treatment response and long-term dentofacial adaptations to maxillary expansion and protraction. *Semin. Orthod.* **3,** 255–264 (1997).

7. Ge, Y. S., Liu, J., Chen, L., Han, J. L. & Guo, X. Dentofacial effects of two facemask therapies for maxillary protraction. *Angle Orthod.* **82,** 1083–1091 (2012).

8. Franchi, L., Baccetti, T. & McNamara, J. A. Postpubertal assessment of treatment timing for maxillary expansion and protraction therapy followed by fixed appliances. *Am. J. Orthod. Dentofac. Orthop. Off. Publ. Am. Assoc. Orthod. Its Const. Soc. Am. Board Orthod.* **126,** 555–568 (2004).

9. Sung, S. J. & Baik, H. S. Assessment of skeletal and dental changes by maxillary protraction. *Am. J. Orthod. Dentofac. Orthop. Off. Publ. Am. Assoc. Orthod. Its Const. Soc. Am. Board Orthod.* **114,** 492–502 (1998).

10. Yüksel, S., Uçem, T. T. & Keykubat, A. Early and late facemask therapy. *Eur. J. Orthod.* **23,** 559–568 (2001).

11. Nanda, R. Protraction of maxilla in rhesus monkeys by controlled extraoral forces. *Am. J. Orthod.* **74,** 121–141 (1978).

12. Nanda, R. & Hickory, W. Zygomaticomaxillary suture adaptations incident to anteriorly-directed forces in rhesus monkeys. *Angle Orthod.* **54,** 199–210 (1984).

13. McNamara, J. A. An orthopedic approach to the treatment of Class III malocclusion in young patients. *J. Clin. Orthod. JCO* **21,** 598–608 (1987).

14. Melsen, B. & Melsen, F. The postnatal development of the palatomaxillary region studied on human autopsy material. *Am. J. Orthod.* **82,** 329–342 (1982).

15. Cha, K.-S. Skeletal changes of maxillary protraction in patients exhibiting skeletal class III malocclusion: a comparison of three skeletal maturation groups. *Angle Orthod.* **73,** 26–35 (2003).

16. Enacar, A., Giray, B., Pehlivanoglu, M. & Iplikcioglu, H. Facemask therapy with rigid anchorage in a patient with maxillary hypoplasia and severe oligodontia. *Am. J. Orthod. Dentofac. Orthop. Off. Publ. Am. Assoc. Orthod. Its Const. Soc. Am. Board Orthod.* **123,** 571–577 (2003).

17. Kokich, V. G., Shapiro, P. A., Oswald, R., Koskinen-Moffett, L. & Clarren, S. K. Ankylosed teeth as abutments for maxillary protraction: a case report. *Am. J. Orthod.* **88,** 303–307 (1985).

18. Baccetti, T., McGill, J. S., Franchi, L., McNamara, J. A. & Tollaro, I. Skeletal effects of early treatment of Class III malocclusion with maxillary expansion and face-mask therapy. *Am. J. Orthod. Dentofac. Orthop. Off. Publ. Am. Assoc. Orthod. Its Const. Soc. Am. Board Orthod.* **113,** 333–343 (1998).

19. Singer, S. L., Henry, P. J. & Rosenberg, I. Osseointegrated implants as an adjunct to facemask therapy: a case report. *Angle Orthod.* **70,** 253–262 (2000).

20. Kircelli, B. H. & Pektas, Z. O. Midfacial protraction with skeletally anchored face mask therapy: a novel approach and preliminary results. *Am. J. Orthod. Dentofac. Orthop. Off. Publ. Am. Assoc. Orthod. Its Const. Soc. Am. Board Orthod.* **133,** 440–449 (2008).

21. Cevidanes, L., Baccetti, T., Franchi, L., McNamara, J. A. & De Clerck, H. Comparison of two protocols for maxillary protraction: bone anchors versus face mask with rapid maxillary expansion. *Angle Orthod.* **80,** 799–806 (2010).

22. Mao, J. J., Wang, X. & Kopher, R. A. Biomechanics of craniofacial sutures: orthopedic implications. *Angle Orthod.* **73,** 128–135 (2003).

23. Lee, H., Ting, K., Nelson, M., Sun, N. & Sung, S.-J. Maxillary expansion in customized finite element method models. *Am. J. Orthod. Dentofac. Orthop. Off. Publ. Am. Assoc. Orthod. Its Const. Soc. Am. Board Orthod.* **136,** 367–374 (2009).

24. Tanne, K. & Sakuda, M. Biomechanical and clinical changes of the craniofacial complex from orthopedic maxillary protraction. *Angle Orthod.* **61,** 145–152 (1991).

25. Yu, H. S., Baik, H. S., Sung, S. J., Kim, K. D. & Cho, Y. S. Three-dimensional finite-element analysis of maxillary protraction with and without rapid palatal expansion. *Eur. J. Orthod.* **29,** 118–125 (2007).

26. Burnett, D. S. *Finite element analysis: from concepts to applications*. (Addison-Wesley Pub. Co, 1987).

27. Reddy, J. N. *An introduction to the finite element method*. (McGraw-Hill Higher Education, 2006).

28. *The Finite Element Method in Engineering*. (Butterworth-Heinemann, 2011). at <http://www.myilibrary.com?id=96441>

29. Cattaneo, P. M., Dalstra, M. & Melsen, B. The finite element method: a tool to study orthodontic tooth movement. *J. Dent. Res.* **84,** 428–433 (2005).

30. Gautam, P., Valiathan, A. & Adhikari, R. Maxillary protraction with and without maxillary expansion: a finite element analysis of sutural stresses. *Am. J. Orthod. Dentofac. Orthop. Off. Publ. Am. Assoc. Orthod. Its Const. Soc. Am. Board Orthod.* **136,** 361–366 (2009).

31. Mehta, B. V., Rajani, S. & Sinha, G. Comparison of image processing techniques (Magnetic resonance imaging, computed tomography scan and ultrasound) for 3D modeling and analysis of the human bones. *J. Digit. Imaging* **10,** 203–206 (1997).

32. Takhounts, E. G. *et al.* Investigation of traumatic brain injuries using the next generation of simulated injury monitor (SIMon) finite element head model. *Stapp Car Crash J.* **52,** 1–31 (2008).

33. Kraft, R. H., McKee, P. J., Dagro, A. M. & Grafton, S. T. Combining the finite element method with structural connectome-based analysis for modeling neurotrauma: connectome neurotrauma mechanics. *PLoS Comput. Biol.* **8,** e1002619 (2012).

34. Wright, R. M. & Ramesh, K. T. An axonal strain injury criterion for traumatic brain injury. *Biomech. Model. Mechanobiol.* **11,** 245–260 (2012).

35. Horgan, T. J. & Gilchrist, M. D. Influence of FE model variability in predicting brain motion and intracranial pressure changes in head impact simulations. *Int. J. Crashworthiness* **9,** 401–418 (2004).

36. El Sayed, T., Mota, A., Fraternali, F. & Ortiz, M. Biomechanics of traumatic brain injury. *Comput. Methods Appl. Mech. Eng.* **197,** 4692–4701 (2008).

37. Chen, Y. & Ostoja-Starzewski, M. MRI-based finite element modeling of head trauma: spherically focusing shear waves. *Acta Mech.* **213,** 155–167 (2010).

38. White, S. C. & Pharoah, M. J. *Oral radiology: principles and interpretation*. (2014). at <http://www.contentreserve.com/TitleInfo.asp?ID={2DA229B6-2960-4260-AC4B-4E7920F02A73}&Format=50>

39. Young, P. G. *et al.* An efficient approach to converting three-dimensional image data into highly accurate computational models. *Philos. Transact. A Math. Phys. Eng. Sci.* **366,** 3155–3173 (2008).

40. Moaveni, S. *Finite element analysis: theory and application with ANSYS*. (Pearson Prentice Hall, 2008).

41. ANSYS. 4.72 SOLID72 3-D 4-Node Tetrahedral Structural Solid with Rotations (UP19980821). at <http://www.ansys.stuba.sk/html/elem_55/chapter4/ES4-72.htm>

42. Tanne, K., Matsubara, S. & Sakuda, M. Location of the centre of resistance for the nasomaxillary complex studied in a three-dimensional finite element model. *Br. J. Orthod.* **22,** 227–232 (1995).

43. Jeon, P. D., Turley, P. K., Moon, H. B. & Ting, K. Analysis of stress in the periodontium of the maxillary first molar with a three-dimensional finite element model. *Am. J. Orthod. Dentofac. Orthop. Off. Publ. Am. Assoc. Orthod. Its Const. Soc. Am. Board Orthod.* **115,** 267–274 (1999).

44. Pirelli, P., Ragazzoni, E., Botti, F., Arcuri, C. & Cocchia, D. A comparative light microscopic study of human midpalatal suture and periodontal ligament. *Minerva Stomatol.* **46,** 429–433 (1997).

45. Lagravère, M. O., Carey, J., Ben-Zvi, M., Packota, G. V. & Major, P. W. Effect of object location on the density measurement and Hounsfield conversion in a NewTom 3G cone beam computed tomography unit. *Dento Maxillo Facial Radiol.* **37,** 305–308 (2008).

46. Lee, K. G., Ryu, Y. K., Park, Y. C. & Rudolph, D. J. A study of holographic interferometry on the initial reaction of maxillofacial complex during protraction. *Am. J. Orthod. Dentofac. Orthop. Off. Publ. Am. Assoc. Orthod. Its Const. Soc. Am. Board Orthod.* **111,** 623–632 (1997).

47. Hino, C. T. *et al.* Three-dimensional analysis of maxillary changes associated with facemask and rapid maxillary expansion compared with bone anchored maxillary protraction. *Am. J. Orthod. Dentofac. Orthop. Off. Publ. Am. Assoc. Orthod. Its Const. Soc. Am. Board Orthod.* **144,** 705–714 (2013).

48. Almeida, R. R. de *et al.* Management of the Class III malocclusion treated with maxillary expansion, facemask therapy and corrective orthodontic. A 15-year follow-up. *J. Appl. Oral Sci. Rev. FOB* **23,** 101–109 (2015).